Inorg. Chem. **2005**, *44*, 1763–1773

Two Novel Iron(II) Materials Based on Dianionic N_4O_2 Schiff Bases: Structural Properties and Spin-Crossover Characteristics in the Series [Fe(3-X,5-NO_2-sal-N(1,4,7,10)] (X = H, 3-MeO, 3-EtO)

Lionel Salmon, Azzedine Bousseksou, Bruno Donnadieu, and Jean-Pierre Tuchagues*

Laboratoire de Chimie de Coordination, UPR CNRS 8241, 205 route de Narbonne, 31077 Toulouse Cedex 04, France

Received November 16, 2004

Two spin-crossover (SCO) complexes [Fe^{II}(3-MeO,5-NO_2-sal-N(1,4,7,10)] (**1**) and [Fe^{II}(3-EtO,5-NO_2-sal-N(1,4,7,-10)] (**2**) have been prepared and studied (3-MeO,5-NO_2-sal-N(1,4,7,10) and 3-EtO,5-NO_2-sal-N(1,4,7,10) are deprotonated 2-[12-(hydroxy-3-methoxy-5-nitrophenyl)-2,5,8,11-tetraazadodeca-1,11-dien-1-yl]-2-methoxy-4-nitrophenol and 2-[12-(hydroxy-3-ethoxy-5-nitrophenyl)-2,5,8,11-tetraazadodeca-1,11-dien-1-yl]-2-ethoxy-4-nitrophenol, respectively). The X-ray diffraction analysis of complex **1** ($C_{22}H_{26}N_6O_8Fe$) evidenced the same *Pbnb* orthorhombic system at 160 K (high-spin (HS) state) and 100 K (low-spin (LS) state). At 160 K, $a = 8.4810(9)$ Å, $b = 14.7704(14)$ Å, $c = 18.769(2)$ Å, $V = 2351.2(4)$ Å^3, and $Z = 4$. At 100 K, $a = 8.5317(8)$ Å, $b = 14.4674(15)$ Å, $c = 18.814(2)$ Å, and $V = 2322.2(4)$ Å^3. Complex **2** ($C_{28}H_{38}N_6O_9Fe$) crystallizes in the $P\bar{1}$ triclinic system. At 160 K (HS state), $a = 10.265(4)$ Å, $b = 10.861(4)$ Å, $c = 14.181(5)$ Å, $\alpha = 84.18(4)°$, $\beta = 70.53(5)°$, $\gamma = 88.95(5)°$, $V = 1482.6(10)$ Å^3, and $Z = 2$. The iron(II) coordination sphere is distorted octahedral in **1** and **2** with a cis-α arrangement of the N_4O_2 donor set of the hexadentate ligand. The molecules are connected into 1D infinite chains through hydrogen contacts involving the secondary amine functions and O_{nitro} atoms of the ligands in adjacent molecules. Investigation of their magnetic properties and Mössbauer spectra has revealed very different SCO behaviors: complex **1** exhibits a cooperative SCO without residual LS or HS fraction; complex **2** shows a LS ↔ HS SCO involving ~5% of the Fe^{II} ions in the 30–150 K range. The phenomenological cooperative interaction parameter $J = 138$ K evaluated from the area of the hysteresis loop indicates a cooperative effect weaker in **1** than in [Fe^{II}(5NO_2-sal-N(1,4,7,10))]. The theoretical approach to the SCO in **2** indicates a HS ground state and a LS first excited level 53 K above: the thermal dependence of the system occurs through population of vibrational states. Comparison of the structural and electronic properties of the ferrous SCO materials with parent N_4O_2 ligands shows that the properties of SCO are closely related to intermolecular interactions and crystal packing.

Introduction

The growing interest in molecular and supramolecular materials stems from the functions they may exhibit, as the result of the electronic structure of the constituent molecules.[1] Fascinating topics in this area of contemporary chemistry include molecular magnetic materials[2] and bistable molecular materials based on the temperature-, pressure-, or light-induced high-spin (HS) ↔ low-spin (LS) crossover of their metal centers.[3] For such an assembly of spin-crossover (SCO) molecules, magnetic and optical properties may switch within a minute range of external perturbation (temperature, pressure, light, or magnetic field) when cooperative intermolecular interactions lead to the occurrence of hysteresis (first-order SCO), which endows the material with memory.[4] The

* To whom correspondence should be addressed. E-mail: tuchague@lcc-toulouse.fr. Tel.: (33) 561 333154. Fax: (33) 561 553003.

(1) See for example: (a) *Molecular Magnetism: From Molecular Assemblies to the Devices*; O'Connor, C. J., Coronado, E., Delhaès, P., Gatteschi, D., Miller, J. S., Eds.; NATO ASI Series, Series E; Kluwer Academic Publishers: Dordrecht, The Netherlands, 1996; Vol. 321. (b) Ohkoshi, S.; Hashimoto, K. *J. Am. Chem. Soc.* **1999**, *121*, 10591. (c) Coronado, E.; Galan-Mascaros, J. R.; Gomez-Garcia, C. J.; Laukhin, V. *Nature* **2000**, *408*, 447. (d) Takamatsu, N.; Akutagawa, T.; Hasegawa, T.; Nakamura, T.; Inabe, T.; Fujita, W.; Awaga, K. *Inorg. Chem.* **2000**, *39*, 870. (e) Irie, M. *Chem. Rev.* **2000**, *100*, 1685. (f) Dearden, A. L.; Parsons, S.; Winpenny, R. E. P. *Angew. Chem., Int. Ed.* **2001**, *40*, 151. (g) Itkis, M. E.; Chi, X.; Cordes, A. W.; Haddon, R. C. *Science* **2002**, *296*, 1443. (h) Irie, M.; Fukaminato, T.; Sasaki, T.; Tamai, N.; Kawai, T. Nature **2002**, *420*, 759. (i) Halder, G. J.; Kepert, C. J.; Moubaraki, B.; Murray, K. S.; Cashion, J. D. *Science* **2002**, *298*, 1762. (j) Miller, J. S. *Angew. Chem., Int. Ed.* **2003**, *42*, 27. (k) Tasiopoulos, A. J.; Vinslava, A.; Wernsdorfer, W.; Christou, G.; *Angew. Chem., Int. Ed.* **2004**, *43*, 2117.

10.1021/ic048387k CCC: $30.25
Published on Web 02/09/2005

most important class of bistable SCO molecules belongs to the category of octahedral iron(II) compounds:[5] their SCO involves change in population of the e_g and t_{2g} orbitals with LS and HS states characterized by a large difference in spin quantum numbers ($S = 0$ (LS), and $S = 2$ (HS). Strong cooperativity resulting in first-order SCO may be reached through two strategies which are currently explored, the polymeric and supramolecular approaches.[6] The polymeric approach consists of synthesizing 1D, 2D, or 3D polymeric materials resulting from coordination of Fe^{2+} cations to bridging ligands suitable for generating LS and HS ligand fields in the ranges appropriate for iron(II) SCO.[7] The supramolecular approach consists of synthesizing mononuclear SCO units containing various functional vectors able to lead to condensed materials (hydrogen bonding, π stacking, ...).[8] Several SCO materials have already been obtained through this promising approach,[9] and the paramount role of the "communication wires" resulting from the type of functional vectors used has been unambiguously illustrated in a recent study.[10] In this contribution, we report on two novel spin-crossover ferrous materials [Fe(3-MeO,5-NO_2-sal-N(1,4,7,10)] (**1**) and [Fe(3-EtO,5-NO_2-sal-N(1,4,7,-10)] (**2**). The novel N_4O_2 dianionic ligands involved in **1** and **2** are the deprotonated forms of 2-[12-(hydroxy-3-methoxy-5-nitrophenyl)-2,5,8,11-tetraazadodeca-1,11-dien-1-yl]-2-methoxy-4-nitrophenol and 2-[12-(hydroxy-3-ethoxy-5-nitrophenyl)-2,5,8,11-tetraazadodeca-1,11-dien-1-yl]-2-ethoxy-4-nitrophenol, respectively. A parent dianionic Schiff base with N_4O_2 donor set (2-[12-(hydroxy-5-nitrophenyl)-2,5,8,11-tetraazadodeca-1,11-dien-1-yl]-4-nitrophenol, 5-NO_2-sal-N(1,4,7,10)) is known to yield a ferrous material in which the thermally induced first-order SCO occurs in two steps separated by a 35 K plateau where 50% of LS and HS Fe^{2+} sites are present.[9a] Compound **1** exhibits a thermally induced first-order SCO occurring in one step while compound **2** undergoes a gradual and incomplete LS $\leftrightarrow$ HS SCO. To thoroughly analyze these behaviors, we describe the crystal structure of **1** at 160 K (HS state) and 100 K (LS state) and the crystal structure of **2** at 160 K (HS state). We also report on the temperature-dependent magnetic properties and Mössbauer spectra of both materials. Finally, we compare the crystal structures and physical properties of [Fe(5-NO_2-sal-N(1,4,7,10)],[9a] **1**, and **2** to identify the specific structural and electronic parameters responsible for the impressive differences in SCO behavior among these closely related materials.

Experimental Section

Materials. 3-Ethoxy-2-hydroxybenzaldehyde, 3-methoxy-2-hydroxy-5-nitrobenzaldehyde, methylamine, sodium dithionite, sodium

(2) See for example: (a) Gatteschi, D.; Sessoli, R.; Cornia, A. *J. Chem. Soc., Chem. Commun.* **2000**, 725. (b) Christou, G.; Gatteschi, D.; Hendrickson, D. N.; Sessoli, R. *MRS Bull.* **2000**, *25*, 66. (c) Andres, H.; Basler, R.; Blake, A. J.; Cadiou, C.; Chaboussant, G.; Grant, C. M.; Güdel, H.-U.; Murrie, M.; Parsons, S.; Paulsen, C.; Semadini, F.; Villar, V.; Wernsdorfer, W.; Winpenny, R. E. P. *Chem.—Eur. J.* **2002**, *8*, 4867. (d) Sokol, J. J.; Hee, A. G.; Long, J. R. *J. Am. Chem. Soc.* **2002**, *124*, 7656. (e) Gatteschi, D.; Sessoli, R. *Angew. Chem., Int. Ed.* **2003**, *42*, 268. (f) Berlinguette, C. P.; Vaughn, D.; Cañada-Vilalta, C.; Galán-Mescarós, J. R.; Dunbar, K. R. *Angew. Chem., Int. Ed.* **2003**, *42*, 1523. (g) Dendrinou-Samara, C.; Alexiou, M.; Zaleski, C. M.; Kampf, J. W.; Kirk, M. L.; Kessissoglou, D. P.; Pecoraro, V. L. *Angew. Chem., Int. Ed.* **2003**, *42*, 3763. (h) Murrie, M.; Teat, S. J.; Stoeckli-Evans, H.; Güdel, H. U. *Angew. Chem., Int. Ed.* **2003**, *42*, 4653. (i) Ishikawa, N.; Sugita, M.; Ishikawa, T.; Koshihara, S.; Kaizu, Y. *J. Am. Chem. Soc.* **2003**, *125*, 8694. (j) Osa, S.; Kido, T.; Matsumoto, N.; Re, N.; Pochaba, A. *J. Am. Chem. Soc.* **2004**, *126*, 420. (k) Boudalis, A. K.; Donnadieu, B.; Nastopoulos, V.; Clemente-Juan, J. M.; Mari, A.; Sanakis, Y.; Tuchagues, J.-P.; Perlepes, S. P. *Angew. Chem., Int. Ed.* **2004**, *43*, 2266.

(3) See for example: (a) Gütlich, P.; Hauser, A.; Spiering, H. *Angew. Chem., Int. Ed. Engl.* **1994**, *33*, 2024. (b) Kahn, O. *Curr. Opin. Solid State Mater. Sci.* **1996**, *1*, 547. (c) Gütlich, P.; Garcia, Y.; Woike, T. *Coord. Chem. Rev.* **2001**, 219−221, 839. (d) Bousseksou, A.; Molnár, G.; Tuchagues, J.-P.; Menéndez, N.; Codjovi, E.; Varret, F. *C. R. Chim.* **2003**, *6*, 329. (e) Real, J. A.; Gaspar, A. B.; Niel, V.; Muñoz, M. C. *Coord. Chem. Rev.* **2003**, *236*, 121. (f) Bousseksou, A.; Varret, F.; Goiran, M.; Boukheddaden, K.; Tuchagues, J.-P. In *Spin Crossover in Transition Metal Compounds III*; Gütlich, P., Goodwin, H. A., Eds.; Topics in Current Chemistry; Springer: Berlin, 2004; Vol. 235, pp 65−84 and references therein.

(4) See for example: (a) Kahn, O.; Launay, J. P. *Chemtronics* **1988**, *3*, 140. (b) Gütlich, P.; Hauser, A. *Coord. Chem. Rev.* **1990**, *97*, 1. (c) Kahn, O.; Kröber, J.; Jay, C. *Adv. Mater.* **1992**, *4*, 718. (d) Jay, C.; Grolière, F.; Kahn, O.; Kröber, J. *Mol. Cryst. Liq. Cryst.* **1993**, *A234*, 255. (e) Gütlich, P. *Nucl. Instrum. Methods Phys. Res.* **1993**, *B76*, 387. (f) Kahn, O.; Martinez, C. J. *Science* **1998**, *279*, 44. (g) Hauser, A.; Jeftic, J.; Romstedt, H.; Hinek, R.; Spiering, H. *Coord. Chem. Rev.* **1999**, *190−192*, 471. (h) Hayami, S.; Gu, Z.-Z.; Yoshiki, H.; Fujishima, A.; Sato, O. *J. Am. Chem. Soc.* **2000**, *123*, 11644. (i) Sunatsuki, Y.; Ikuta, Y.; Matsumoto, N.; Ohta, H.; Kojima, M.; Iijima, S.; Hayami, S.; Maeda, Y.; Kaizaki, S.; Dahan, F.; Tuchagues, J.-P. *Angew. Chem., Int. Ed.* **2003**, *42*, 1614.

(5) See for example: *Magnetism: A Supramolecular Function*; Kahn, O., Ed.; NATO ASI Series, Series C; Kluwer Academic Publ.: Dordrecht, The Netherlands, 1996; Vol. 284,

(6) (a) Lemercier, G.; Verelst, M.; Bousseksou, A.; Varret, F.; Tuchagues, J.-P. In *Magnetism: A Supramolecular Function*; Kahn, O., Ed.; NATO ASI Series, Series C; Kluwer Academic Publishers: Dordrecht, Thje Netherlands, 1996; Vol. 484, p 335. (b) Kahn, O.; Garcia, Y.; Létard, J. F.; Mathonière, C. In *Supramolecular Engineering of Synthetic Metallic Materials, Conductors and Magnets*; Veciana, J., Rovira, C., Amabilino, D. B., Eds.; NATO ASI Series, Series C; Kluwer Academic Publishers: Dordrecht, The Netherlands, 1998; Vol. 518, p 127.

(7) (a) Garcia, Y.; Kahn, O.; Rabardel, L.; Chansou, B.; Salmon, L.; Tuchagues, J.-P. *Inorg. Chem.* **1999**, *38*, 4663 and refs 17−32 therein. (b) van Konningsbruggen, P. J.; Garcia, Y.; Kahn, O.; Fournes, L.; Kooijman, H.; Spek, A. L.; Haasnoot, J. G.; Moscovici, J.; Provost, K.; Michalowicz, A.; Renz, F.; Gütlich, P. *Inorg. Chem.* **2000**, *39*, 1891. (c) Moliner, N.; Muñoz, C.; Letard, S.; Solans, X.; Menendez, N.; Goujon, A.; Varret, F.; Real, J. A. *Inorg. Chem.* **2000**, *39*, 5390. (d) Reger, D. L.; Little, C. A.; Rheingold, A. L.; Lam, M.; Liable-Sands, L. M.; Rhagitan, B.; Concolino, T.; Mohan, A.; Long, G. J.; Briois, V.; Grandjean, F. *Inorg. Chem.* **2001**, *40*, 1508. (e) Niel, V.; Thompson, A. L.; Muñoz, M. C.; Galet, A.; Goeta, A. E.; Real, J. *Angew. Chem., Int. Ed.* **2003**, *42*, 3760. (f) Grunert, C. M.; Schweifer, J.; Weinberger, P.; Linert, W.; Mereiter, K.; Hilscher, G.; Wiesinger, G.; van Koningsbruggen, P. J. *Inorg. Chem.* **2004**, *43*, 155.

(8) (a) Vogtle, F. *Supramolecular Chemistry*; Wiley: New York, 1991. (b) *Transition Metals in Supramolecular Chemistry*; Fabbrizzi, L., Poggi, A., Eds.; Nato ASI Series; Kluwer Academic Publishers: Dordrecht, The Netherlands, 1994. (c) Lehn, J.-M. *Supramolecular Chemistry*; VCH: Weinheim, Germany, 1995.

(9) (a) Boinnard, D.; Bousseskou, A.; Dworkin, A.; Savariault, J. M.; Varret, F.; Tuchagues, J.-P. *Inorg. Chem.* **1994**, *33*, 271. (b) Bousseksou, A.; Tommasi, L.; Lemercier, G.; Varret, F.; Tuchagues, J.-P. *Chem. Phys. Lett.* **1995**, *243*, 493. (c) Létard, J. F.; Guionneau, P.; Codjovi, E.; Lavastre, O.; Bravic, G.; Chasseau, D.; Kahn, O. *J. Am. Chem. Soc.* **1997**, *119*, 10861. (d) Létard, J. F.; Guionneau, P.; Rabardel, L.; Howard, J. A. K.; Goeta, A. E.; Chasseau, D.; Kahn, O. *Inorg. Chem.* **1998**, *37*, 4432. (e) Zhong, Z. J.; Tao, J. Q.; Yu, Z.; Dun, C. Y.; Liu, Y. J.; You, X. Z. *J. Chem. Soc., Dalton Trans.* **1998**, 327. (f) Hayami, S.; Gu, Z.-Z.; Shiro, M.; Einaga, Y.; Sato, O. *J. Am. Chem. Soc.* **2000**, *122*, 7126. (g) Ikuta, Y.; Ooidemizu, M.; Yamahata, Y.; Yamada, M.; Osa, S.; Matsumoto, N.; Iijima, S.; Sunatsuki, Y.; Kojima, M.; Dahan, F.; Tuchagues, J.-P. *Inorg. Chem.* **2003**, *42*, 7001. (h) Yamada, M.; Ooidemizu, M.; Ikuta, Y.; Osa, S.; Matsumoto, N.; Iijima, S.; Kojima, M.; Dahan, F.; Tuchagues, J.-P. *Inorg. Chem.* **2003**, *42*, 8406.

(10) (a) Salmon, L.; Donnadieu, B.; Bousseksou, A.; Tuchagues J.-P. *C. R. Acad. Sci. Paris* **1999**, *2c*, 305. (b) Sunatsuki, Y.; Ohta, H.; Kojima, M.; Ikuta, Y.; Goto, Y.; Matsumoto, N.; Iijima, S.; Akashi, H.; Kaizaki, S.; Dahan, F.; Tuchagues, J.-P. *Inorg. Chem.* **2004**, *43*, 4154.

hydroxide (Aldrich), triethylenetetramine, and triethylenetetramine dihydrochloride (Fluka) were used as purchased. High-grade solvents used for the synthesis of complexes were distilled prior to use. Iron(II) acetate dihydrate was synthesized as previously described.[11]

Ligands. 3-Ethoxy-2-hydroxy-5-nitrobenzaldehyde was prepared through nitration of 3-ethoxy-2-hydroxybenzaldehyde.[12] 2-Methoxy-6-[(methylimino)methyl]-4-nitrophenol was prepared through Schiff base condensation of methylamine with 3-methoxy-2-hydroxy-5-nitrobenzaldehyde in methanol.

Complexes. All complexation reactions and sample preparations for physical measurements were carried out in a purified nitrogen atmosphere within a glovebox (Vacuum Atmospheres H.E.43.2) equipped with a dry-train (Jahan EVAC 7).

Fe(2-methoxy-6-[(methylimino)methyl]-4-nitrophenoxo)$_2$-(H$_2$O)$_2$ (P1). An equimolar amount of solid NaOH was added to a solution of 2-methoxy-6-[(methylimino)methyl]-4-nitrophenol (400 mg, 1.9 mmol) in MeOH (4 mL). The resulting deprotonated ligand solution was stirred for 30 min prior to addition of a methanolic solution of iron acetate dihydrate (200 mg, 0.95 mmol) in methanol (3 mL). A brown precipitate formed before the end of the iron acetate addition. The slurry was stirred for 24 h at room temperature; the precipitate was filtered off, washed with 5 mL of methanol, and dried under vacuum. Yield: 410 mg; 85%. Anal. Calcd (found) for $C_{18}H_{22}N_4O_{10}Fe$: C, 44.22 (43.63); H, 3.45 (3.41); N, 11.08 (10.98). Characteristic IR absorptions (KBr, cm^{-1}): 1632 s, $\nu_{C=N}$; 1558 s, ν_{NO_2} (as); 1319 s, ν_{NO_2} (s).

[Fe(3-MeO,5-NO$_2$-sal-N(1,4,7,10)] (1). The preparation of complex **1** was adapted from a transimination method.[13] A 4-fold excess of triethylenetetramine dihydrochloride was mixed with the precursor complex **P1** (200 mg, 0.39 mmol) in methanol (4 mL). The slurry was stirred for 48 h at room temperature, and the resulting microcrystalline powder was filtered off, washed with methanol, and dried under vacuum. The final compound was obtained as a dark-green microcrystalline powder. Single-crystals suitable for X-ray measurement were obtained by slow interdiffusion of solutions of the intermediate complex **P1** and triethylenetetramine dihydrochloride. Yield: 190 mg; 87%. Anal. Calcd (found) for $FeC_{22}H_{26}N_6O_8$: C, 46.23 (46.72); H, 4.50 (4.66); N, 14.82 (15.06)); Fe, 9.74 (10.01). Characteristic IR absorptions (KBr, cm^{-1}): 3296 m, ν_{NH}; 2920−2853, ν_{CH}; 1623 s, $\nu_{C=N}$; 1561 s, ν_{NO_2} (as); 1284 s, ν_{NO_2} (s).

Fe(3-ethoxy-2-hydroxo-5-nitrobenzaldehyde)$_2$(H$_2$O)$_2$ (P2). An equimolar amount of solid NaOH and 0.5 equiv of solid sodium dithionite were successively added to a solution of 3-ethoxy-2-hydroxy-5-nitrobenzaldehyde (300 mg, 1.42 mmol) in MeOH (3 mL). The resulting deprotonated ligand solution was stirred for 30 min prior to addition of a methanolic solution of iron acetate dihydrate (150 mg, 0.71 mmol) in methanol (3 mL). A brown precipitate formed before the end of the iron acetate addition. The slurry was stirred for 24 h at room temperature; the precipitate was filtered off, washed with 5 mL of methanol, and dried under vacuum. Yield: 400 mg; 95%. Anal. Calcd (found) for $C_{18}H_{20}N_2O_{12}Fe$: C, 36.53 (36.20); H, 3.13 (3.31); N, 4.53 (4.47). Characteristic IR absorptions (KBr, cm^{-1}): 1635 s, $\nu_{C=O}$; 1563 s, ν_{NO_2} (as); 1322 s, ν_{NO_2} (s).

[Fe(3-EtO,5-NO$_2$-sal-N(1,4,7,10)] (2). The preparation of complex **2** was adapted from a general method.[14] An equimolar amount of triethylenetetramine was mixed with the precursor complex **P2** (400 mg, 0,78 mmol) in methanol (3 mL). The slurry was stirred for 24 h at room temperature; the resulting microcrystalline powder was filtered off, washed with methanol, and dried under vacuum. The final compound was obtained as a green powder. Subsequent crystallization of the resulting green powder from thf/Et_2O yielded well-shaped dark green single-crystals. Yield: 290 mg; 64%. Anal. Calcd (found) for $FeC_{24}H_{30}N_6O_8$: C, 48.68 (49.16); H, 4.64 (5.12); N, 13.99 (14.34); Fe 9.53 (8.80). Characteristic IR absorptions (KBr, cm^{-1}): 3295 m, ν_{NH}; 2978−2871, ν_{CH}; 1631 s, $\nu_{C=N}$; 1561 s, ν_{NO_2} (as); 1289 s, ν_{NO_2} (s).

Crystallographic Data Collection and Structure Determination. The selected crystal was pasted on a glass fiber and mounted on a Stoe imaging plate diffraction system (IPDS) using a graphite-monochromated Mo Kα radiation and equipped with an Oxford Cryostream cooler device. The data were collected at 160 and 100 K (**1**) and 160 K (**2**). Final unit cell parameters were obtained by least-squares refinement of a set of 5000 reflections. No significant fluctuations of diffracted intensities were observed during the measurements. A total of 15 313 (**1**, 160 K), 15 001 (**1**, 100 K), and 9204 (**2**) reflections were collected. Totals of 1879 (R_{int} = 0.040) (**1**, 160 K), 1840 (R_{int} = 0.080) (**1**, 100 K), and 3378 (R_{int} = 0.1815) (**2**) independent reflections were used in the refinements.

The structures were solved by direct methods using SHELXS-97[15] and refined by least-squares procedures on F_o^2 with SHELXL-97[16] by minimizing the function $\Sigma w(F_o^2 - F_c^2)^2$, where F_o and F_c are respectively the observed and calculated structure factors. The atomic scattering factors were taken from ref 17. All atoms were located on difference Fourier maps. All non-hydrogen atoms were refined anisotropically. All hydrogen atoms were found on difference Fourier syntheses. Except for the H atoms of the secondary amine functions which were refined isotropically, H atoms were introduced in calculations with the riding model and U_{iso}(H) 10% higher than that of the riding atom. Weighted R-factors wR and goodness of fit S are based on F_o^2; conventional R-factors R are based on F_o, with F_o set to zero for negative F_o^2. Drawings of the molecules were performed with the program ZORTEP[18] with 50% of probability displacement ellipsoids for non-hydrogen atoms. Crystal data collection and refinement parameters are given in Table 1, and selected bond distances and angles are gathered in Tables 2 and 3.

Physical Measurements. Elemental analyses were carried out at the Laboratoire de Chimie de Coordination Microanalytical Laboratory in Toulouse, France, for C, H, and N and at the Service central de Microanalyses du CNRS in Vernaison, France, for Fe. IR spectra were recorded on a Perkin-Elmer 983 spectrophotometer coupled with a Perkin-Elmer infrared data station. Samples were run as KBr pellets prepared under nitrogen in the drybox.

Mössbauer measurements were obtained on a constant-acceleration conventional spectrometer with a 50 mCi source of ^{57}Co (Rh matrix). Isomer shift values (δ) throughout the paper are given with respect to metallic iron at room temperature. The absorber was a

(11) Boinnard, D.; Cassoux, P.; Petrouleas, V.; Savariault, J.-M.; Tuchagues, J.-P. *Inorg. Chem.* **1990**, *29*, 4114.
(12) Davies, W.; Rubenstein, L. *J. Chem. Soc.* **1923**, *123*, 2850.
(13) Carbonaro, L.; Giacomelli, A.; Senatore, L.; Valli, L. *Inorg. Chim. Acta* **1989**, *165*, 197.
(14) De Vries, J. L. K. F.; Trooster, j. M.; de Boer, E. *J. Chem. Soc. D* **1970**, *10*, 604−605.
(15) Sheldrick, G. M. *SHELXS-97, Program for Crystal Structure Solution*; University of Göttingen: Göttingen, Germany, 1990.
(16) Sheldrick, G. M. *SHELXL-97, Program for the Refinement of Crystal Structure*; University of Göttingen: Göttingen, Germany, 1997.
(17) *International Tables for Crystallography*; Kluwer Academic Publishers: Dordrecht, The Netherlands, 1992; Vol. C, Tables 4.2.6.8 and 6.1.1.4.
(18) Zolnaï, L. *ZORTEP, Graphical Program for X-ray Structures Analysis*; University of Heildelberg: Heildelberg, Germany, 1998.

Table 1. Crystallographic Data for [Fe(3-MeO,5-NO_2-sal-N(1,4,7,10))] (**1**) and [Fe(3EtO,5NO_2-Sal-N(1,4,7,10))]·THF (**2**·THF)

	1 (160 K)	**1** (100 K)	**2**·THF
formula	$C_{22}H_{26}N_6O_8Fe$	$C_{22}H_{26}N_6O_8Fe$	$C_{28}H_{38}N_6O_9Fe$
fw	558.34	558.34	658.49
space group	*Pbnb* (No. 56)	*Pbnb* (No. 56)	$P\bar{1}$ (No. 2)
a, Å	8.4810(9)	8.5317(8)	10.265(4)
b, Å	14.7704(14)	14.4674(15)	10.861(4)
c, Å	18.769(2)	18.814(2)	14.181(5)
α, deg	90	90	84.18(4)
β, deg	90	90	70.53(5)
γ, deg	90	90	88.95(5)
V, Å^3	2351.2(4)	2322.2(4)	1482.6(10)
Z	4	4	2
temp, K	160	100	160
λ, Å	0.710 73	0.710 73	0.710 73
ρ(calcd), g cm^{-3}	1.577	1.597	1.475
μ, mm^{-1}	0.704	0.713	0.573
R1[a]	0.0293	0.0476	0.0998
wR2(F^2)[b]	0.0728	0.1052	0.2045

[a] $R1 = \Sigma||F_o| - |F_c||/\Sigma|F_o|$. [b] $wR2 = \{\Sigma[w(F_o^2 - F_c^2)^2]/\Sigma[w(F_o^2)^2]\}^{1/2}$.

sample of 100 mg of microcrystalline powder enclosed in a 20 mm diameter cylindrical plastic sample folder, the size of which had been determined to optimize the absorption. Variable-temperature spectra were obtained in the 80−300 K range, by using a MD 306 Oxford cryostat, the thermal scanning being monitored by an Oxford ITC4 servocontrol device (±0.1 K accuracy). A least-squares computer program[19] was used to fit the Mössbauer parameters and determine their standard deviations of statistical origin (given in parentheses).

Variable-temperature magnetic susceptibility data were obtained as previously described on polycrystalline samples with a Faraday-type magnetometer equipped with a continuous-flow Oxford Instruments cryostat[20] (**1**, 77−290 K) and a Quantum Design MPMS SQUID susceptometer (**2**, 4−300 K).[21] Diamagnetic corrections were applied by using Pascal's constants.

Results

Syntheses. While the generic 2-[12-(hydroxy-5-nitrophenyl)-2,5,8,11-tetraazadodeca-1,11-dien-1-yl]-4-nitrophenol ligand (5-NO_2-sal-N(1,4,7,10)) was cleanly obtained by the usual Schiff base condensation reaction,[22] attempts to similarly prepare and isolate 2-[12-(hydroxy-3-methoxy-5-nitrophenyl)-2,5,8,11-tetraazadodeca-1,11-dien-1-yl]-2-methoxy-4-nitrophenol (3-MeO,5-NO_2-sal-N(1,4,7,10)) and 2-[12-(hydroxy-3-ethoxy-5-nitrophenyl)-2,5,8,11-tetraazadodeca-1,11-dien-1-yl]-2-ethoxy-4-nitrophenol (3-EtO,5-NO_2-sal-N(1,4,7,10)) did not yield pure samples of the expected hexadentate ligands. As previously reported in the case of unsubstituted salicylaldehyde,[23] a tris-condensation reaction occurs involving, in addition to the two terminal primary amine functions of triethylenetetramine, both secondary amine functions in the formation of a central imidazolidine ring. While the tris-condensation is predominant with unsubstituted salicylaldehyde, the bis-condensation largely predominates with 5-nitrosalicylaldehyde, and mixtures of Schiff bases resulting from the simultaneous bis- and tris-condensation of triethylenetetramine with the corresponding 3,5-disubstituted salicylaldehydes are obtained. The relative ratio of bis- and tris-Schiff bases depends on the reaction conditions and substituents on the aromatic rings of the salicylaldehyde reactant.[24] To overcome this difficulty, several synthetic routes have been used which allow preparing metal complexes without prior isolation of the corresponding hexadentate bis-Schiff bases.[23] In the case of 3-ethoxy-2-hydroxy-5-nitrobenzaldehyde, the one-pot reaction and the method using a precursor metal complex with triethylenetetramine failed. The only route yielding pure samples of complex **2** consisted in reacting the Fe(3-ethoxy-2-hydroxo-5-nitrobenzaldehyde)$_2$(H_2O)$_2$ precursor complex (**P2**) with triethylenetetramine. In the case of 3-methoxy-2-hydroxy-5-nitrobenzaldehyde, all methods described above failed, and pure samples of complex **1** could only be obtained through transimination of the Fe(2-methoxy-6-[(methylimino)methyl]-4-nitrophenoxo)$_2$(H_2O)$_2$ precursor complex (**P1**) with triethylenetetramine dihydrochloride, an original method inspired from the work of Carbonaro et al.[13] The above-mentioned precursor complexes **P1** and **P2** have not been previously described.

Description of the Structures. The molecular structure of complex **1** was solved at two temperatures, namely 160 and 100 K where all Fe^{2+} ions are in the HS and LS states, respectively. The same space group, *Pbnb* is retained: there is no crystallographic phase transition. The molecular entity shown in Figure 1 (160 K) illustrates how the dianionic hexadentate Schiff base ligand wraps the iron(II) center in the cis-α mode with coordination of the six donor atoms (N_4O_2) in a distorted octahedral geometry.

Selected bond lengths and angles for the 160 and 100 K structures are gathered in Table 2: they are typical of HS Fe^{II} at 160 K, and of LS Fe^{II} at 100 K.

The main structural modification concerns the iron(II) coordination sphere and results in a 1.2% decrease in volume of the unit cell between 160 and 100 K. The prominent features of the structure at both temperatures result from (i) the location of the iron on a 2-fold symmetry axis, (ii) the location of the inversion center between two adjacent molecules, and (iii) the presence of two glide planes which allows one to describe the unit cell ($Z = 4$) with half a molecule. As shown in Figure 2, the molecules are organized into infinite 1D chains owing to a dense network of hydrogen contacts linking the central secondary amine functions of each complex molecule to the terminal 5-nitro groups of the adjacent molecules (N2···O3 = 3.40 Å, N2···O4 = 3.24 Å) through the H(N2) atom (H(N2)···O3 = 2.63 Å, H(N2)···O4 = 2.42 Å). As mentioned in the case of [Fe(5-NO_2-sal-N(1,4,7,10))],[9a] Δ and Λ enantiomorphs alternate along a chain.

(19) Varret, F. *Proceedings of the International Conference on Mössbauer Effect Applications*; Jaipur, India, 1981; Indian National Science Academy: New Delhi, 1982.
(20) Luneau, D.; Savariault, J.-M.; Cassoux, P.; Tuchagues, J.-P. *J. Chem. Soc., Dalton Trans.* **1988**, 1225.
(21) Bousseksou, A.; Verelst, M.; Constant-Machado, H.; Lemercier, G.; Tuchagues, J.-P.; Varret, F. *Inorg. Chem.* **1996**, *35*, 110.
(22) Mabad, B.; Cassoux, P.; Tuchagues, J.-P.; Hendrickson, D. N. *Inorg. Chem.* **1986**, *25*, 1420.
(23) (a) Mukherjee, A. K. *Sci. Cult.* **1953**, *19*, 107. (b) Das Sarma, B.; Bailar, J. C., Jr. *J. Am. Chem. Soc.* **1954**, *76*, 4051. (c) Das Sarma, B.; Bailar, J. C., Jr. *J. Am. Chem. Soc.* **1955**, *77*, 5476.
(24) Thiel, A.; Salmon, L.; Tuchagues, J.-P. Unpublished results.

Scheme 1. Synthetic Pathways to Complexes **1** and **2**

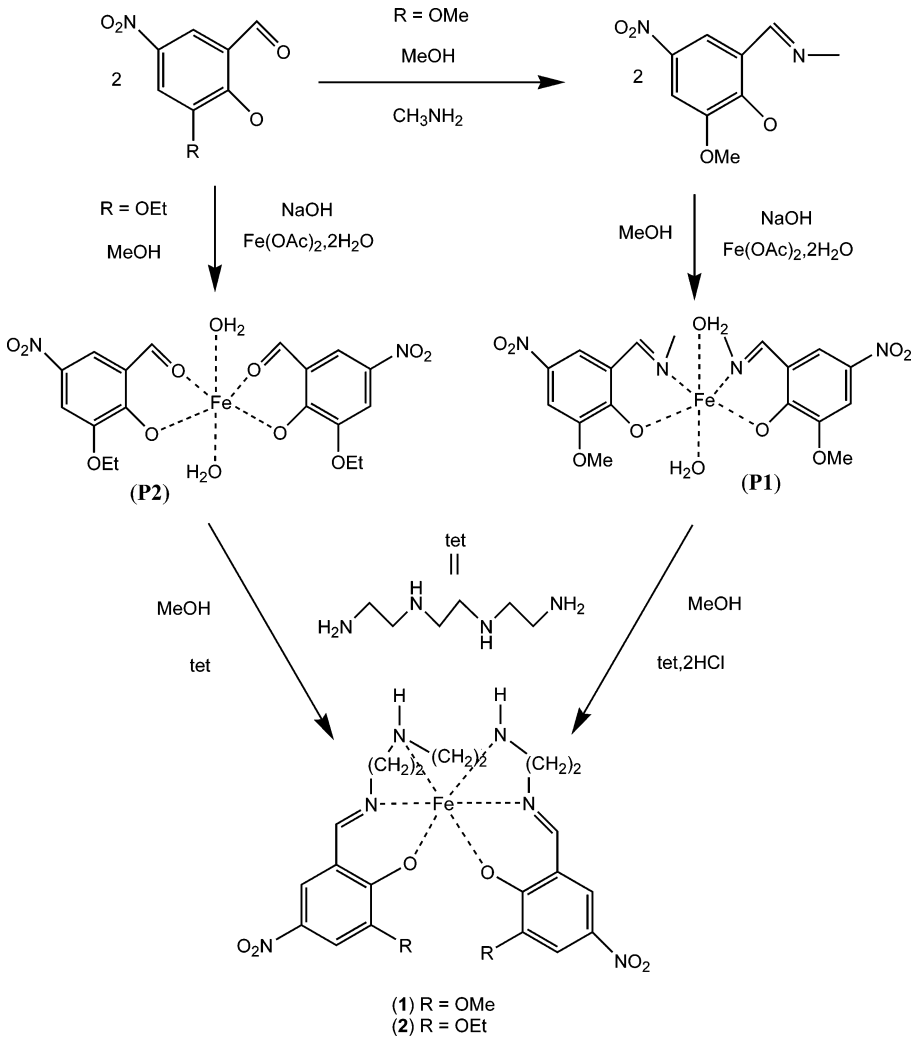

As shown in Figure 3, the infinite chains, piled up along *b* with a *b*/2 separation, alternately develop along two directions crossing at 49° with respect to each other and at ±49°/2 with respect to the *c* direction.

The molecular structure of complex **2** was solved at 160 K where all Fe^{2+} ions are in the HS state. The complex molecule shown in Figure 4 illustrates that the ligand environment afforded by this parent dianionic hexadentate

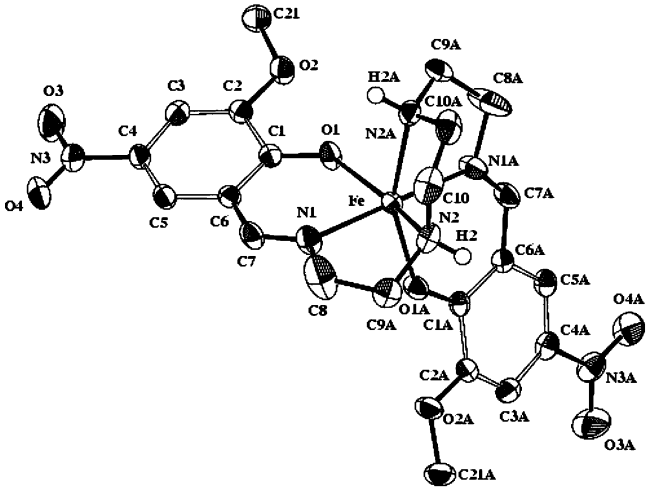

Figure 1. ORTEP view of [Fe(3-MeO,5-NO_2-sal-N(1,4,7,10))] (**1**) with atom-numbering scheme showing 50% probability ellipsoids.

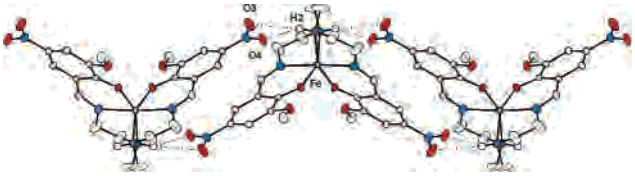

Figure 2. Chain of hydrogen-bonded molecules of [Fe(3-MeO,5-NO_2-sal-N(1,4,7,10))] (**1**).

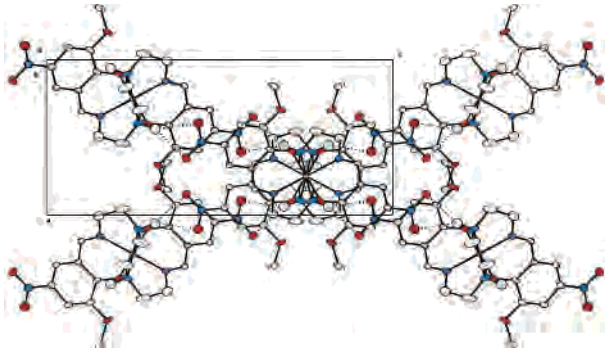

Figure 3. Two chains of [Fe(3-MeO,5-NO_2-sal-N(1,4,7,10))] (**1**) alternately developing along two directions crossing at ±49°/2 with respect to the *c* direction.

Table 2. Selected Interatomic Distances (Å) and Angles (deg) for [Fe(3-MeO,5-NO_2-sal-N(1,4,7,10))] (**1**) at 160 K (HS) and 100 K (LS)[a]

	160 K	100 K		160 K	100 K
Fe(1)−O(1)	2.0445(14)	1.993(3)	Fe(1)−N(1)	2.1272(18)	2.015(3)
Fe(1)−N(2)	2.2150(19)	2.101(3)	O(1)−Fe−O(1′)	109.73(9)	104.09(15)
O(1)−Fe−N(1)	84.90(6)	88.19(12)	O(1)−Fe−N(1′)	93.13(7)	90.34(12)
O(1)−Fe−N(2)	155.43(7)	163.65(13)	O(1)−Fe−N(2′)	88.85(7)	88.42(12)
N(1)−Fe−N(1′)	176.59(11)	177.6(2)	N(1)−Fe−N(2)	77.96(7)	81.15(15)
N(1)−Fe−N(2′)	104.75(8)	100.70(15)	N(2)−Fe−N(2′)	78.80(11)	81.48(19)

[a] Symmetry operation: $' = -x + 1/2, y, -z + 1/2$.

Table 3. Selected Interatomic Distances (Å) and Angles (deg) for [Fe(3-EtO,5-NO_2-sal-N(1,4,7,10))]·THF (**2**·THF) at 160 K (HS)

Fe−O(1)	2.061(3)	Fe−N(1)	2.139(5)	Fe−N(3)	2.211(6)
Fe−O(2)	2.013(5)	Fe−N(2)	2.219(5)	Fe−N(4)	2.125(5)
O(1)−Fe−O(2)	108.24(18)	O(1)−Fe−N(1)	84.04(17)	O(1)−Fe−N(2)	151.44(19)
O(1)−Fe−N(3)	86.36(18)	O(1)−Fe−N(4)	92.92(17)	O(2)−Fe−N(1)	90.1(2)
O(2)−Fe−N(2)	93.6(2)	O(2)−Fe−N(3)	158.35(18)	O(2)−Fe−N(4)	84.7(2)
N(1)−Fe−N(2)	77.57(18)	N(1)−Fe−N(3)	107.6(2)	N(1)−Fe−N(4)	172.9(2)
N(2)−Fe−N(3)	78.8(2)	N(2)−Fe−N(4)	107.56(18)	N(3)−Fe−N(4)	78.5(2)

Schiff base is extremely similar to that in complex **1**. Selected bond lengths and angles are gathered in Table 3: they are typical of HS Fe^{II}.

At variance with the case of **1**, the iron is not located on any special position, but the location of the inversion center between two adjacent molecules is again responsible for alternation of Δ and Λ enantiomorphic molecules. As shown in Figure 5, the molecules are organized into pseudo 1D chains along [011] owing to hydrogen contacts linking the central secondary amine functions of each complex molecule to the terminal 5-nitro groups of the adjacent molecules (N2···O6 = 3.09 Å, N3···O5 = 3.43 Å) through the H(N2) and H(N3) atoms (H(N2)···O6 = 2.17 Å, H(N3)···O5 = 2.69 Å).

However, three significant differences between the networks of hydrogen contacts in **2** compared to **1** deserve to be mentioned: (i) In complex **2**, each nitro group participates only in one hydrogen contact with the facing amine function while it participates in two hydrogen contacts with the facing amine function in complex **1**. (ii) In complex **2**, very weak hydrogen contacts (N3···O5) alternate with stronger ones (N2···O6) along the chains while the pairs of hydrogen contacts (N2···O3 and N2···O4) are identical along the chains of complex **1**. (iii) In complex **2**, all chains run along [011] and weak N3···O5 contacts (3.31 Å) connect chains adjacent along *a* through H(N3) (Figure 6) while their stacking-up along *b* does not involve any hydrogen contact.

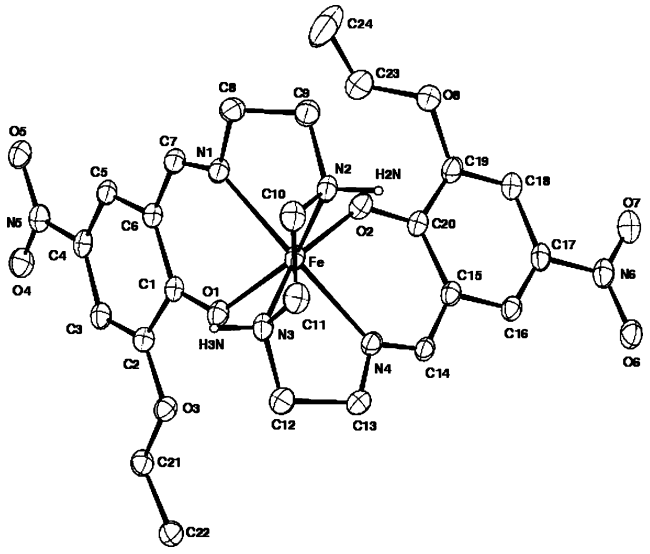

Figure 4. ORTEP view of [Fe(3-EtO,5-NO_2-sal-N(1,4,7,10))]·THF (**2**·THF) with atom-numbering scheme showing 50% probability ellipsoids.

Magnetic Studies. The thermal dependence of the $\chi_M T$ product where χ_M is the molar magnetic susceptibility of [Fe(3-MeO,5-NO_2-sal-N(1,4,7,10))] (**1**) is plotted in Figure 7.

At room temperature, $\chi_M T$ is equal to 3.81 cm^3 K mol^{-1}, which is at the upper limit of the range of values expected for HS iron(II). As the temperature is lowered below room temperature, $\chi_M T$ first remains constant, then steeply decreases between 127 and 120 K, and finally remains nearly constant and equal to 0.45 cm^3 K mol^{-1} below 120 K. When the 77 K minimum temperature is reached, the temperature variation is reversed to the heating mode, yielding a $\chi_M T$ versus *T* plot perfectly similar to that obtained in the cooling mode but shifted by 4 K toward higher temperatures (open circles in Figure 7). In the cooling mode the temperature of the spin-transition $T_{1/2}\downarrow$ is 125 K ($\chi_M T = 2.052$ cm^3 K mol^{-1}), and $T_{1/2}\uparrow$ equals 129 K in the warming mode. Such a thermal hysteresis is characteristic of a first-order SCO. The high values of $\chi_M T$ in the whole temperature range result from minute aerial oxidation to iron(III) during transfer of the sample from the glovebox as evidenced by Mössbauer spectroscopy (see below).

The thermal dependence of the $\chi_M T$ product of [Fe(3-EtO,5-NO_2-sal-N(1,4,7,10))]·THF (**2**·THF) plotted in Figure 8 shows two inflections located near 170 and 60 K, which delineate segments characterized by different slopes. In the 300−170 K range, $\chi_M T$ is practically constant (3.305−3.285 cm^3 K mol^{-1}), the $\chi_M T$ decrease is larger in the 170−60 K range (3.285−3.227 cm^3 K mol^{-1}), a small χ_MT increase then occurs in the 60−30 K range (3.227−3.247 cm^3 K mol^{-1}), and finally a significant $\chi_M T$ lowering (3.247−2.709 cm^3 K mol^{-1}) characterizes the 30−4 K low-temperature range. The $\chi_M T$ value at 300 K is slightly larger than the spin-only value

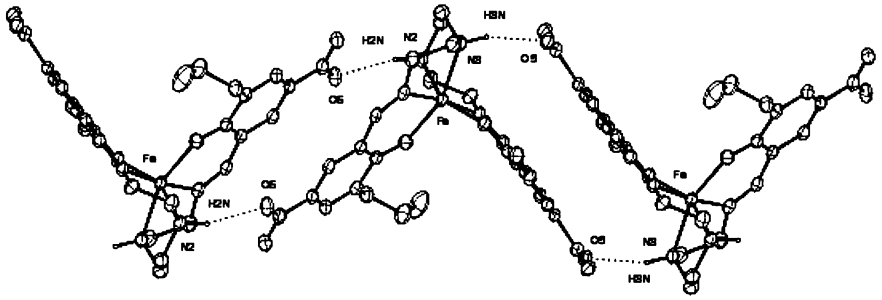

Figure 5. Chain of hydrogen-bonded molecules of [Fe(3-EtO,5-NO_2-sal-N(1,4,7,10))]·THF (**2**·THF).

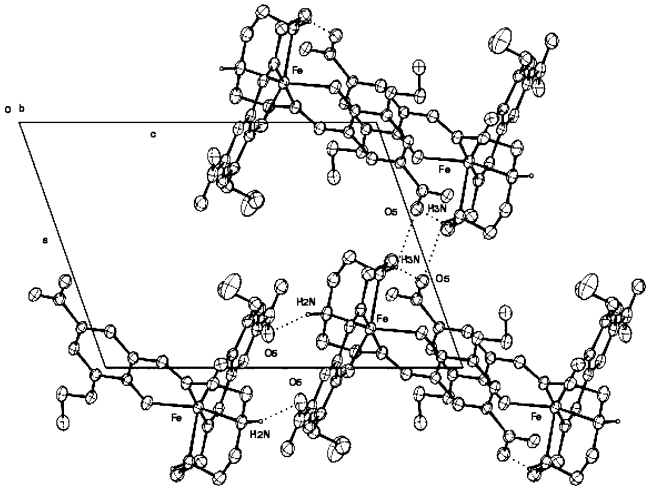

Figure 6. Chains of [Fe(3-EtO,5-NO_2-sal-N(1,4,7,10))]·THF (**2**·THF) running along [011] through H(N3) and weak N3−H···O5 contacts (3.31 Å) connecting chains adjacent along a.

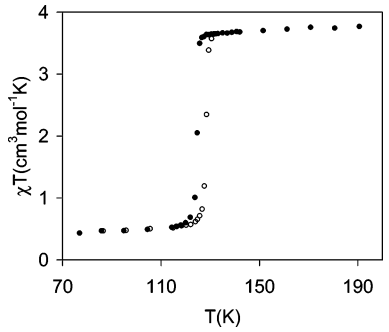

Figure 7. Thermal variation of the $\chi_M T$ product for [Fe(3-MeO,5-NO_2-sal-N(1,4,7,10))] (**1**) in the cooling (●) and heating (○) modes.

for $S = 2$ as usually observed for high-spin iron(II) complexes. The very small thermal dependence of $\chi_M T$ in the first segment (300−170 K) can be related to this phenomenon. On the other hand, the larger thermal dependence of $\chi_M T$ in the low-temperature range (25−4 K) indicates the presence of zero-field splitting of the high-spin iron(II) ground state and possibly operation of weak intermolecular antiferromagnetic interactions mediated by the network of hydrogen contacts characterizing this structure. The small thermal dependence of $\chi_M T$ in the intermediate segments (170−30 K) may originate from an HS ↔ LS crossover.[21,25]

Mössbauer Spectroscopy. Representative Mössbauer spectra of [Fe(3-MeO,5-NO_2-sal-N(1,4,7,10))] (**1**) recorded in the cooling mode are shown in Figure 9, and values of

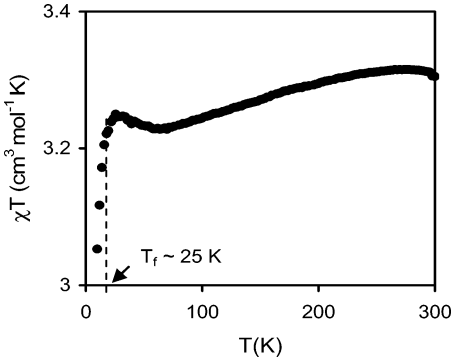

Figure 8. Thermal variation of the $\chi_M T$ product for [Fe(3-EtO,5-NO_2-sal-N(1,4,7,10))]·THF (**2**·THF).

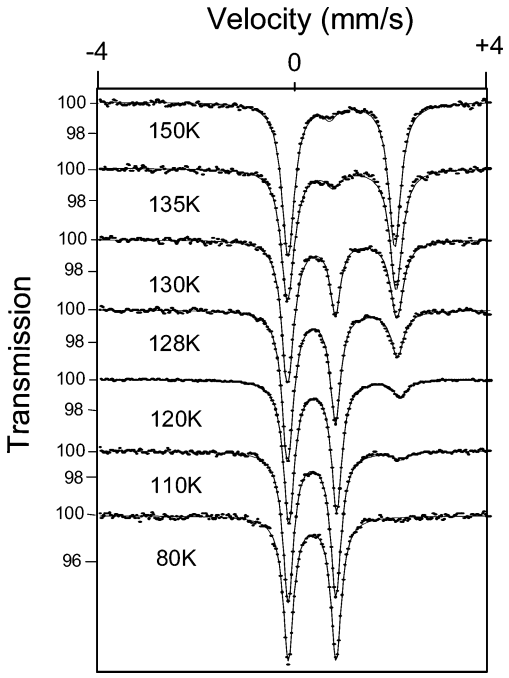

Figure 9. Representative Mössbauer spectra of Fe(3-MeO,5-NO_2-sal-N(1,4,7,10))] (**1**) obtained in the cooling mode.

the Mössbauer parameters obtained by least-squares fitting of the spectra are gathered in Table 4.

At room temperature, the Mössbauer spectrum consists of a unique quadrupole-split doublet, with an isomer shift $\delta = 0.82(9)$ mm s^{-1} and a quadrupole spitting $\Delta E_Q = 1.9(2)$ mm s^{-1}. These parameters are typical of HS iron(II). Below 140 K, a LS iron(II) doublet appears: its parameters are δ

(25) Bousseksou, A.; Constant-Machado, H.; Varret, F. *J. Phys. I* **1995**, *5*, 747.

Table 4. Representative Least-Squares-Fitted Mössbauer Data for [Fe(3-MeO,5-NO_2-sal-N(1,4,7,10))] (**1**)[a]

	low-spin state			high-spin state			
T (K)	δ	ΔE_Q^{LS}	$\Gamma/2$	δ	ΔE_Q^{HS}	$\Gamma/2$	A_{HS}/A_{tot} (%)
293				0.82(9)	1.9(2)	0.131(1)	100
240				0.859(3)	1.971(6)	0.138(2)	100
200				0.881(2)	2.021(4)	0.142(1)	100
160				0.901(1)	2.086(2)	0.144(1)	100
150				0.905(1)	2.103(2)	0.146(2)	100
140	*0.3*	*0.95*	0.15(2)	0.916(1)	2.114(2)	0.150(1)	98.9(5)
137	*0.3*	*0.95*	0.15(2)	0.917(1)	2.122(2)	0.152(2)	97.8(5)
135	*0.3*	*0.95*	0.15(2)	0.918(1)	2.128(2)	0.151(2)	94.6(6)
130	0.305(2)	0.967(3)	0.121(2)	0.943(2)	2.112(2)	0.153(4)	61.4(5)
128	0.315(1)	0.953(2)	0.125(1)	0.952(3)	2.11(6)	0.151(4)	35.5(4)
125	0.321(1)	0.945(2)	0.125(1)	0.952(3)	2.109(9)	0.157(4)	28(4)
120	0.324(1)	0.943(1)	0.124(1)	0.979(4)	2.123(7)	0.164(5)	14.7(3)
115	0.324(1)	0.945(2)	0.123(1)	1.00(1)	2.10(2)	0.14(1)	11.2(8)
110	0.329(1)	0.938(1)	0.127(1)	0.98(2)	2.14(4)	0.14(2)	5.7(5)
100	0.333(1)	0.939(1)	0.125(1)	1.18(4)	2.03(7)	0.30(6)	3.2(8)
90	0.334(1)	0.939(1)	0.127(1)				0
80	0.334(1)	0.939(1)	0.125(1)				0

[a] Isomer shifts (δ, mm s^{-1}) refer to metallic iron at room temperature; ΔE_Q = quadrupole splitting (mm s^{-1}); $\Gamma/2$ = half-width of the lines (mm s^{-1}). Statistical standard deviations are given in parentheses; italicized values were fixed for the fit.

= 0.305(2) mm s^{-1} and ΔE_Q = 0.967(3) mm s^{-1} at 130 K. The high-temperature (T > 150 K) and low-temperature (T < 90 K) spectra evidence the absence of residual LS and HS fractions, respectively.[26] At each temperature the high-spin molar fraction, n_{HS}, may be deduced from the area ratio A_{HS}/A_{tot} determined from the least-squares fitting of the spectra (A_{HS} = area of the HS doublet; A_{tot} = total Mössbauer absorption). In agreement with the results deduced from the magnetic data (Figure 7), the n_{HS} versus T variation in Table 4 confirms the occurrence of a one-step SCO. The step is centered at $T_{1/2}$ = 125 K and very steep.

A study of the thermal variation of the recoil-free fraction of the system has been carried out through a least-squares fitting procedure of A_{tot}[27] allowing one to obtain the Debye temperatures ΘD_{LS} = 215 K and ΘD_{HS} = 160 K. The temperature dependence of ln A_{Tot} derived from the above-mentioned measurements is displayed in Figure 10. The SCO induces an appreciable discontinuity in the slope resulting from different Debye temperatures for the HS and LS forms.

The thermal variation of ΔE_Q(HS) is shown in Figure 11. The 1.90−2.03 mm s^{-1} range of ΔE_Q(HS) values indicates that the local symmetry is lower than cubic and the ground orbital state is rather a doublet (in a well-isolated singlet case, ΔE_Q is in the 3−4 mm s^{-1} range). The small ΔE_Q(HS) variation in this temperature range is characteristic of a strongly distorted octahedral environment as already evidenced by the X-ray crystal structure determinations. It is possible to roughly assess the average energy δ of the excited orbital states belonging to the cubic triplet (insert in Figure 11) assuming that the ΔE_Q(HS) slope varies as δ^{-1}.[28] The slope $d\Delta E_Q(HS)/dT$ can be determined by linear regressions as -1.392×10^{-3} mms^{-1} K^{-1} yielding, as

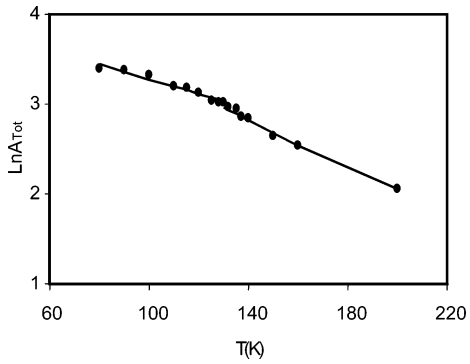

Figure 10. Thermal variation of ln A_{Tot} derived from the Mössbauer spectra of Fe(3-MeO,5-NO_2-sal-N(1,4,7,10))] (**1**). The solid straight lines represent the fits allowing one to obtain the Debye temperatures ΘD_{LS} and ΘD_{HS}.

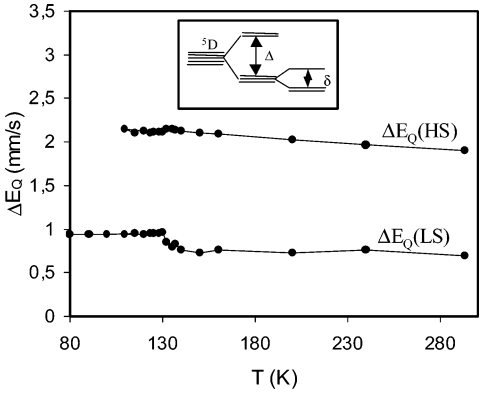

Figure 11. Thermal variation of ΔE_Q(HS) and ΔE_Q(LS) for Fe(3-MeO,5-NO_2-sal-N(1,4,7,10))] (**1**). The insert depicts the ligand-field splitting of the HS state.

(26) All Mössbauer spectra of compound **1** show an additional doublet, the relative ratio of which (~5%) remains constant in the whole temperature range (80−293 K). A careful observation of Figure 9 shows a very weak component between the two components of the LS doublet in the 80 and 135 K spectra: this is the high velocity component of the above-mentioned additional doublet. In view of its parameters, this additional doublet has been attributed to the presence of ~5% iron(III), resulting from aerial oxidation during transfer of the Mössbauer sample (enclosed in a sample holder sealed with paraffin) from the glovebox to the spectrometer. Consequently, this minority iron(III) contribution has been subtracted prior to evaluation of A_{HS}/A_{tot} from each Mössbauer spectrum (Table 4).

(27) Claude, R.; Real, J. A.; Zarembowitch, J.; Kahn, O.; Ouahab, L.; Grandjean, D.; Boukheddaden, K.; Varret, F.; Dworkin, A. *Inorg. Chem.* **1990**, *29*, 4442.

(28) Ducouret-Cérèze, A.; Varret, F. *J. Phys. (Paris)* **1988**, *49*, 661.

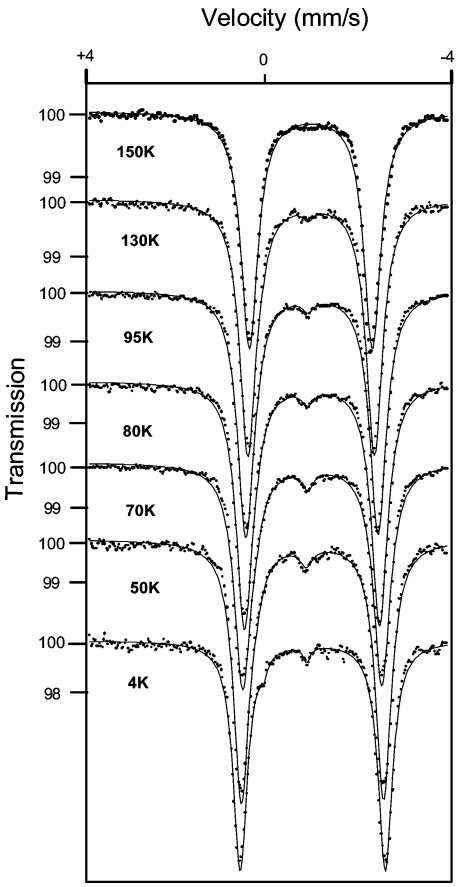

Figure 12. Representative Mössbauer spectra of Fe(3-EtO,5-NO_2-sal-N(1,4,7,10))]·THF (**2**·THF) obtained in the cooling mode.

expected, a δ value ($\sim$1900 cm^{-1}) larger than that obtained for [Fe(5-NO_2-sal-N(1,4,7,10))] ($\sim$1530 cm^{-1}).[9a] The thermal variation of the quadrupole splitting of the LS doublet ΔE_Q(LS) is shown in Figure 11.

In keeping with the isotropic properties of the $^1A_{1g}$ electronic state, the ΔE_Q(LS) values (0.939−0.967 mm s^{-1}) are significantly lower than the ΔE_Q(HS) values. However the relative large ΔE_Q(LS) values confirm the high distortion of the iron local symmetry. In keeping with the assumption that ΔE_Q is a good parameter for exploring local symmetries and their transitions, Figure 11 clearly shows that the thermal variation of ΔE_Q(LS) and ΔE_Q(HS) exhibit a discontinuity around 130 K (associated with the SCO). The linear thermal variation of the isomer shift of the two doublets (not shown) follows the second order Doppler effect law.[29]

Representative Mössbauer spectra of [Fe(3-EtO,5-NO_2-sal-N(1,4,7,10))]·THF (**2**·THF) are shown in Figure 12. The majority high-temperature doublet (110 K) and the weak low-temperature doublet (80 K) are typical of iron(II) in the HS and LS states, respectively. The isomer shift (δ_{HS} = 1.063 and δ_{LS} = 0.38 mm s^{-1}) and quadrupole splitting values (ΔE_Q(HS) = 2.815 and ΔE_Q(LS) = 1.12 mm s^{-1}) are in agreement with those previously reported for iron(II) SCO compounds.

Detailed values of the Mössbauer parameters resulting from the least-squares fitting procedures are listed in Table 5, and the resulting thermal variation of n_{HS} is shown in Figure 13. These data evidence a very gradual 5% thermal variation of the proportion of HS molecules between 30 and 150 K. Below 30 K, the proportion of high-spin molecules remains constant. The same smooth variation is observed by magnetic measurements (Figure 8). The decrease in $\chi_M T$ observed at low temperature which results from zero-field splitting (ZFS) of HS iron(II) is not reflected in the n_{HS} values because Mössbauer spectroscopy is not sensitive to ZFS effect.

Discussion

Compared Application of the Theoretical Approach to Complex 1 and [Fe(5-NO_2-sal-N(1,4,7,10))]. A thermal hysteresis loop is the signature of a first-order SCO.[30] In such a case, the two-level Ising-like model evidences that the phenomenological cooperative interaction parameter is larger than the transition temperature ($|J| > T_{1/2}$).[31] By using this model the area of the hysteresis loop given in Kelvin is approximated by[9b]

$$S \approx 2(|J| - T_{1/2})/\ln(g_{HS}/g_{LS}) \qquad (1)$$

where J is the phenomenological cooperative (ferromagnetic-like) interaction parameter and g_{HS} and g_{LS} are the effective degeneracy ratios accounting for electronic and vibrational levels in the HS and LS spin states, respectively.[21,25,32] The evaluation of the hysteresis loop by using the mean-field treatment[33] is very approximate. However, it may be safely used for relative comparison between two complexes with closely related coordination spheres. The value of the cooperative interaction parameter J obtained with eq 1 and considering the same g_{HS}/g_{LS} ratio (400) as in the case of the two-step SCO complex, [Fe(5-NO_2-sal-N(1,4,7,10))],[9a] is 138 K. Comparison of this value to those previously obtained for the two-step SCO complex (J_1 = 185 K and J_2 = 217 K) suggests a weaker cooperative effect in [Fe(3-MeO,5-NO_2-sal-N(1,4,7,10))] (**1**), in good agreement with the smaller width of the hysteresis loop in this material.

Theoretical Approach to the Spin Equilibrium in Complex 2. The unusually small thermal variation of n_{HS} observed for **2** cannot be interpreted with macroscopic thermodynamic models such as that of Slichter and Drickamer[34] or their Ising-type (i.e. two-level) microscopic equivalents.[30b,32a,33,35] In such a case, a vibrational extension within the macroscopic thermodynamic approach,[36] or its Ising-like counterpart,[25] is required. Following the simplified

(29) Greenwood, N. N.; Gibb, T. C. *Mössbauer Spectroscopy*; Chapman and Hall: London, 1971.
(30) (a) Gütlich, P. *Struct. Bonding* **1981**, *44*, 83. (b) Bousseksou, A.; Nasser, J.; Linares, J.; Boukheddaden, K.; Varret, F. *J. Phys. I* **1992**, *2*, 1331.
(31) Wajnflasz, J.; Pick, R. *J. Phys., Colloq.* **1971**, *32*, C1−91.
(32) (a) Bousseksou, A.; Nasser, J.; Linares, J.; Boukheddaden, K.; Varret, F. *Mol. Cryst. Liq. Cryst*. **1993**, *234*, 269. (b) Bousseksou, A.; Salmon. L.; Varret. F.; Tuchagues, J.-P. *Chem. Phys. Lett.* **1998**, *282*, 209.
(33) Linares, J.; Nasser, J.; Boukheddaden, K.; Varret, F. *J. Magn. Magn. Mater*. **1995**, *140*−*144*, 1507.
(34) (a) Slichter, C. P.; Drickamer, H. G. *J. Chem. Phys.* **1972**, *56*, 2142. (b) Purcell, K. F.; Edward, M. P. *Inorg. Chem.* **1984**, *23*, 2620.
(35) (a) Bousseksou, A.; Nasser, J.; Varret, F. *J. Phys. I* **1993**, *3*, 1463. (b) Wajnflasz, J. *J. Phys.* **1970**, *C40*, 537. (c) Bari, R. A.; Sivardière, J. *J. Phys. Rev. B* **1972**, *5*, 4466.

Table 5. Representative Least-Squares-Fitted Mössbauer Data for [Fe(3-EtO,5-NO_2-sal-N(1,4,7,10))]·THF (**2**·THF)[a]

	low-spin state			high-spin state			
T (K)	δ	ΔE_Q^{LS}	$\Gamma/2$	δ	ΔE_Q^{HS}	$\Gamma/2$	A_{HS}/A_{tot} (%)
293				0.963(2)	2.313(4)	0.203(3)	100
150				1.045((2)	2.656(3)	0.221(3)	100
110	0.38(2)	1.12(7)	*0.13*	1.063(2)	2.815(3)	0.220(3)	97.8
95	0.40(2)	1.12(4)	*0.13*	1.069(2)	2.868(3)	0.217(3)	96.8
80	0.42(2)	1.12(4)	*0.15*	1.072(2)	2.930(4)	0.214(3)	95.8
75	0.40(2)	1.07(4)	0.14(3)	1.077(2)	3.002(4)	0.228(3)	95.3
70	0.42(2)	1.12(4)	0.14(2)	1.078(2)	3.016(4)	0.222(3)	94.9
50	0.40(2)	1.09(4)	0.15(3)	1.083(2)	3.082(4)	0.208(3)	94.6
4	0.45(2)	1.01(4)	0.15(2)	1.090(1)	3.146(3)	0.187(2)	96.7

[a] Isomer shifts (δ, mm s^{-1}) refer to metallic iron at room temperature; ΔE_Q = quadrupole splitting (mm s^{-1}); $\Gamma/2$ = half-width of the lines (mm s^{-1}). Statistical standard deviations are given in parentheses; italicized values were fixed for the fit.

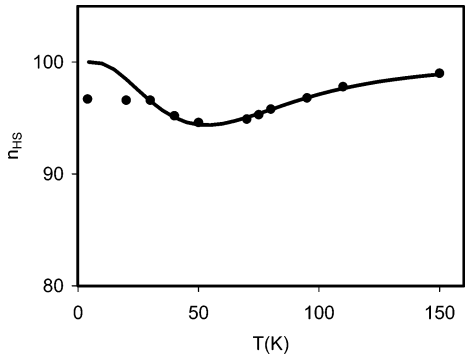

Figure 13. Least-squares fit of the thermal variation of the area ratio A_{HS}/A_{tot} of **2**·THF to the electrovibrational Hamiltonian (1). ● represent the experimental n_{HS} data.

approach based on the Ising-type model, completed with harmonic oscillators associated with the 15 vibrational modes of the coordination octahedron, the partition function associated with the electrovibrational Hamiltonian neglecting cooperative interactions is written in the adiabatic (and harmonic) approximation:

$$ZZ(T) = g_{LSe} ZZ_{vib}{}^{LS}(T) + g_{HSe} ZZ_{vib}{}^{HS}(T)\, e^{-\Delta/k_B T} \quad (2)$$

Here Δ is the electronic energy gap between states of different spin; the electronic degeneracies of the two states, g_{LSe}, g_{HSe}, take the spin-only values (5 and 1 for HS and LS states, respectively) considering that the orbital degeneracy of the $^5T_{2g}$ state is lifted by the low-symmetry components of the ligand field. For each state, the vibrational partition function is written

$$ZZ_{vib}(T) = \prod_{i=1}^{p} Z_{vib}(\omega_i, T) \quad (3)$$

where ω_i is the frequency of the ith vibration mode, characterized by different values in the LS and HS states. $Z_{vib}(\omega_i, T)$ is the partition function of the ith isolated harmonic oscillator (in the LS or HS state).

For simplicity, we have averaged the 15 octahedron distortion modes, assuming a single frequency for each spin state ω_{LS} and ω_{HS} for the LS and HS states, respectively. By thermal averaging, the equilibrium constant of the system ($K_{eq} = n_{HS}/n_{LS}$) is obtained for each temperature leading to $n_{HS}(T)$ as function of temperature. The least-squares fitting of the high-temperature range of the SCO curve ($T > 25$ K) leads to an excellent agreement with the data, as shown in Figure 13. The fitted parameters values are

$$\Delta = 944 \text{ K } (674 \text{ cm}^{-1}); \ \varpi_{LS} = 347 \text{ K } (248 \text{ cm}^{-1}); \ (\omega_{LS}/\omega_{HS}) = 1.62$$

The energies of the electrovibrational levels computed from the above parameter values show that the ground state is HS with a LS first excited level 53 K higher than the HS ground state. With such a small energy difference, the lowest HS and LS states are almost equienergetic and the thermal dependence of the system occurs through population of vibrational levels.

Compared Structural Properties and Bulk Electronic Behavior of the Ferrous Spin-Crossover Materials with N_4O_2 Coordination Spheres. Four SCO complexes in which the N_4O_2 coordination sphere of iron(II) is virtually identical and the individual molecules are similarly connected into 1D infinite chains through the amine functions and nitro groups of adjacent molecules exhibit extremely different bulk electronic behaviors, especially with regard to the cooperativity of their spin transition. In addition to complexes **1** and **2**, fully described in this report, they include [Fe(5-NO_2-sal-N(1,4,7,10))][9a] for which cooperativity results in a first-order two-step SCO and [Fe(3-MeO,5-NO_2-sal-N(1,10)-NMe(4,7))][10a] for which a spin equilibrium with a large residual HS fraction at low temperature is observed.

As evidenced by the molecular structures, the iron(II) coordination sphere is distorted octahedral in the four compounds with an identical cis-α arrangement of the N_4O_2 donor set of the hexadentate ligand including two phenoxo, two imine, and two amine donor atoms. Each type of Fe−L bond spans a narrow range for the four compounds, both in the HS and LS states, Fe−O (HS, 2.055−2.033 Å; LS, 1.994−1.975 Å), Fe−N_{imine} (HS, 2.132−2.122 Å; LS, 2.017−1.985 Å), and Fe−N_{amine} (HS, 2.260−2.215 Å; LS, 2.11−2.09). Thus, except for $T_{1/2}$, the impressively different properties of the SCO in this series cannot be related to the N_4O_2 coordination sphere of iron(II).

In all four compounds, the individual molecules are connected into 1D infinite chains through hydrogen contacts. In [Fe(5-NO_2-sal-N(1,4,7,10))][9a] and complexes **1** and **2**,

(36) Spiering, H.; Meissner, E.; Köppen, H.; Müller, E. W.; Gütlich, P. *Chem. Phys.* **1982**, *68*, 65.

these contacts involve the hydrogen atom of the secondary amine functions and O_{nitro} atoms of the ligands in adjacent molecules. In [Fe(3-MeO,5-NO_2-sal-N(1,10)-NMe(4,7))],[10a] these contacts involve hydrogen atoms of the methyl *N*-amino groups and O_{nitro} atoms of the ligands in adjacent molecules.

(1) Comparison of the SCO properties of [Fe(3-MeO,5-NO_2-sal-N(1,4,7,10))], **1**, and [Fe(3-MeO,5-NO_2-sal-N(1,10)-NMe(4,7))][10a] shows that changing the −N−H···O(nitro)−salicylidene− "communication wire" between adjacent Fe^{II} ions in the 1D chains of a cooperative SCO material to the poorer −N−C−H···O(nitro)−salicylidene− pathway results in a gradual and partial SCO of Fe^{II} in otherwise similar 1D chains of complex molecules. Cooperativity in the SCO phenomenon indeed results from the effectiveness of the intermolecular communication.

(2) Comparison of [Fe(3-MeO,5-NO_2-sal-N(1,4,7,10))], **1**, one-step cooperative SCO ($T_{1/2}$ = 128 K), and [Fe(5-NO_2-sal-N(1,4,7,10))],[9a] two-step cooperative SCO ($T_{1/2}$ = 136 and 173 K), shows that very similar −N−H···O(nitro)−salicylidene− communication wires between adjacent Fe^{II} ions of similar 1D chains may lead to quite different SCO properties. Indeed, while each molecule of [Fe(5-NO_2-sal-N(1,4,7,10))][9a] is linked to the adjacent ones in the chain by two strong N−H···O(nitro) hydrogen bonds (O3···H9 = 2.18 Å, O3···H9−N3 = 153°), in **1** each molecule is linked to the adjacent ones in the chain by four N−H···O(nitro) hydrogen bonds (O3···H2A (O3A···H2) = 2.63 Å, O3···H2A−N2A (O3A···H2−N2) = 146°, O4···H2A (O4A···H2) = 2.42 Å, O4···H2A−N2A (O4A···H2−N2) = 154°). Thus, although the communication wires between adjacent Fe^{II} ions may be slightly more efficient in [Fe(5-NO_2-sal-N(1,4,7,10))][9a] (shorter H-bonds) compared to **1**, this small difference can hardly account for the dramatic increase in communication efficiency implied by the two-step cooperative SCO involving two changes in structural phase of the former compared to the one-step SCO without change of structural phase in **1**. At this point, it is worth comparing the crystal packing of the two materials: all 1D chains of [Fe(5-NO_2-sal-N(1,4,7,10))][9a] run parallel to each other while adjacent chains in the crystal of compound **1** alternately develop along two directions crossing at 49° with respect to each other (Figure 3). Let us consider the LS → HS crossover: expansion of the coordination sphere yields an increase in volume of the individual molecules. This increase implies concerted molecular motions in the direction along which each 1D chain develops. At the crystal level, while these motions result in strains distributed among two directions in compound **1**, they result in strains summed up along the unique direction of all 1D chains in [Fe(5-NO_2-sal-N(1,4,7,10))]. This is typically an elastic phenomenon: while a relatively isotropic elastic constraint can be accommodated by the bulk material (crystal) without essential structural change (**1**), the anisotropic elastic constraint in [Fe(5-NO_2-sal-N(1,4,7,10))] can only be accommodated through a structural phase transition. The same rationale allows to understand why cooperativity of the SCO in polymers increases conversely to dimensionality (3D < 2D < 1D).[7]

(3) Comparison of [Fe(3-MeO,5-NO_2-sal-N(1,4,7,10))], **1**, one-step cooperative SCO ($T_{1/2}$ = 128 K), and [Fe(3-EtO,5-NO_2-sal-N(1,4,7,10))], **2**, gradual and partial (5%) SCO between 30 and 150 K, shows that the N−H···O(nitro) hydrogen contacts in **2** are weaker than in **1** and that they connect adjacent molecules quite differently. Indeed, three significant differences with respect to the hydrogen contacts in **1** indicate that **2** is better described as pairs of hydrogen-bonded molecules interacting very weakly along two different directions with adjacent pairs: (i) In complex **2** each nitro group participates only in one hydrogen contact with the facing amine function, while in complex **1** each nitro group participates in two hydrogen contacts with the facing amine function. (ii) In complex **2**, very weak hydrogen contacts (H(N3)···O5 = 2.69 Å, O5···H−N3 = 143°) alternate with stronger ones (H(N2)···O6 = 2.17 Å, O6···H−N2 = 161°) along pseudo-1D chains, while in complex **1** the pairs of hydrogen contacts (N2···O3 and N2···O4) are identically strong along the chains. (iii) In complex **2**, all chains run along [011] and weak contacts (H(N3)···O5 = 2.60 Å, O5···H−N3 = 133°) connect chains adjacent along *a* (Figure 6).

Concluding Remarks

Taking into account that intermolecular interactions play a paramount role in the cooperativity of the SCO phenomenon,[6,10] it is important to clearly identify how cooperativity is related to which particular structural properties of a material through intermolecular interactions. This is typically a supramolecular problem, and this unique series of supramolecular materials offers an unprecedented opportunity due to the variety of bulk electronic behaviors associated with small chemical and structural changes. The properties of the SCO phenomenon are closely related to intermolecular interactions and crystal packing: (i) Intermolecular interactions determine the effectiveness of communication between adjacent complex molecules and nature of the supramolecular assembly (1D, 2D, or 3D).[7,9] (ii) The crystal packing determines how the elastic constraint resulting from the change in volume of the individual molecules can be accommodated by the crystal upon SCO, either without or with structural phase change according to the isotropic or anisotropic nature of the elastic constraint, respectively.[9,10,37]

Acknowledgment. The European Community is acknowledged for partial support within the framework of the TMR Contract FMRX-CT980199 entitled "Thermal and Optical Switching of Molecular Spin States" (TOSS).

Supporting Information Available: X-ray crystallographic files of [Fe(3-MeO,5-NO_2-sal-N(1,4,7,10))], **1**, and [Fe(3-EtO,5-NO_2-sal-N(1,4,7,10))], **2**, in CIF format. This material is available free of charge via the Internet at http://pubs.acs.org.

IC048387K

(37) König, E. *Prog. Inorg. Chem.* **1987**, *35*, 527.